



## Mapping the surface composition of Europa with SUDA

William Goode<sup>a,\*</sup>, Sascha Kempf<sup>a</sup>, Jürgen Schmidt<sup>b,c</sup>

<sup>a</sup> *LASP, University of Colorado, Boulder, CO, USA*

<sup>b</sup> *Institute of Geological Sciences, Freie Universität Berlin, Germany*

<sup>c</sup> *Space Physics and Astronomy Research Unit, University of Oulu, Finland*



### ARTICLE INFO

#### Keywords:

Europa  
Surface composition  
Geological processes  
Habitability  
Dust analyzers

### ABSTRACT

To assess the potential habitability of Jupiter's moon Europa, it is important to understand its chemical composition (Hand et al., 2007). Young terrain features on Europa's surface likely consist of material up-welled from the liquid water source below (Wilson et al., 1997; Pappalardo et al., 1998; McCord et al., 1999; Figueredo and Greeley, 2004; Mével and Mercier, 2007), encoding relevant compositional information. A major science objective of NASA's Europa Clipper mission is to characterize the composition of young terrain features using data acquired on close flybys. The Surface Dust Analyzer (SUDA) is an in situ instrument that collects and analyzes the composition of individual grains (Kempf et al., 2012), which are ejected from Europa's surface by a continuous bombardment of interplanetary impactors (Krüger et al., 1999, 2003; Goode et al., 2021). By applying a dynamical model of these particles, we compute the probability of SUDA's detections originating from a given feature along the flyby trajectory based on Monte Carlo (MC) simulations. The time-of-flight (TOF) mass spectra that characterize the chemical composition of individual grains, results in a time series of various compositional types along the flyby. We present here a method to analyze a time series of compositional spectra recorded by SUDA that provides a robust estimate for the abundance of compositional types on the surface, spatially resolved for features along the ground track of the flyby. By demonstrating the association of compositional detections with geological sites of origin, data collected by SUDA can be used to infer the compositional ground truth for terrain features on Europa.

## 1. Introduction

Jupiter's ocean world Europa is one of the most compelling places in the solar system to test hypotheses on habitability and search for life (Chyba and Phillips, 2001; Marion et al., 2003; Hand et al., 2007). To determine whether or not Europa is habitable (Marais et al., 2008), we must identify the chemical constituents of the subsurface ocean. To this end, a major science objective for NASA's Europa Clipper mission is to characterize the composition of young geological features on the surface using data collected on close flybys (Lam et al., 2018). These features likely possess material sourced from a subsurface ocean showing high abundances of hydrated salts (Wilson et al., 1997; Pappalardo et al., 1998; McCord et al., 1999; Figueredo and Greeley, 2004; Mével and Mercier, 2007). In this paper, we examine the capability of the Surface Dust Analyzer (SUDA) on Europa Clipper to identify the overall composition of high-priority young features on Europa's surface.

### 1.1. Background

The composition of young terrain features on Europa has remained an active and controversial area of study. Early investigations using data from the Near Infrared Mass Spectrometer (NIMS) aboard the Galileo spacecraft have found the non-water ice component of dark young terrain mainly consists of hydrated salts (McCord et al., 1998, 1999). The water-ice band distortions seen in the NIMS data are well matched by linear mixture models for various species of hydrated salts (Dalton, 2007; Shirley et al., 2010; Prockter et al., 2017). Indeed Prockter et al. (2017) show that younger dark terrain has significantly higher abundances of hydrated salts than older light terrain. However, the specific type(s) of salts present on Europa have yet to be identified. With the current data, the competing hypotheses that the spectra are showing sulfuric acid hydrates (Carlson et al., 2005) cannot be eliminated. Decoupling the abundance of hydrated salts, sulfuric acid, and other non-ice components on Europa's surface will play an important role in identifying the endogenous material emplaced in Europa's young terrain by a subsurface

\* Corresponding author.

E-mail address: [william.goode@colorado.edu](mailto:william.goode@colorado.edu) (W. Goode).

ocean.

Additional investigations using ground-based telescopes (Ligier et al., 2016) and the Hubble Space Telescope (HST) have utilized high spectral resolution near-infrared (NIR) (Brown and Hand, 2013; Hand and Brown, 2013), UV (Trumbo et al., 2022), and visible-wavelength (Trumbo et al., 2020) spectra to investigate the non-ice component of Europa's surface composition. Brown and Hand (2013) hypothesize that the young terrain in the trailing hemisphere contains  $\text{MgSO}_4$ , which they suggest is a product of sulfur radiolysis of  $\text{MgCl}_2$ , NaCl, and KCl endogenously deposited on the surface. Sodium chlorides were identified in the leading hemisphere (Trumbo et al., 2019, 2022) during HST observations using UV and visible-wavelength spectral features, consistent with the irradiation of NaCl, and is spatially correlated with chaos (i.e. young) terrain. Since NaCl,  $\text{MgCl}_2$ , and KCl are difficult to distinguish in the visible and IR spectra, unambiguously identifying such species will likely require in situ analysis of sputtered gas species (Brown and Hand, 2013) or samples ejected directly from the surface by micrometeoroid bombardment (Postberg et al., 2011a; Kempf et al., 2012; Goode et al., 2021).

## 1.2. Application of a Dust Analyzer

Utilizing a dust analyzer enables the identification of surface composition with much higher precision than remote sensing can achieve alone (Kempf et al., 2012). In situ analysis of the composition of material sampled directly from the surfaces of both young and old terrain can distinguish which material is endogenous versus exogenous. Spatially resolving the sites of origin may help constrain whether sulfur-bearing species on the surface originate from a sub-surface ocean or uniquely originate via implantation from Io. The precise nature of compositional species identification by dust analyzers provides a valuable opportunity to make perspicuous measurements regarding the nature of subsurface processes and thereby habitability at Europa.

It is advantageous to identify species and estimate abundances belonging to individual features, particularly those that likely contain material sourced from a sub-surface ocean (Pappalardo and Sullivan, 1996; Pappalardo et al., 1998; Schmidt et al., 2011). Identifying specific compositional species and their relative abundances among different geological features could help constrain the chemistry and conditions beneath the surface (McCord et al., 1999). Hence, it is our goal to know how spatially resolved compositional data acquired by SUDA corresponds to the geology of surface features so that we may better understand their origin and evolution, in particular with respect to what they might tell us about the subsurface ocean. This paper presents the way in which the SUDA data will be acquired during close Europa flybys over terrain features as well as a method for analyzing the time-series of compositional detections along a flyby over a feature in order to infer compositional ground truth.

SUDA acquires compositional data from individual ejected submicron dust and ice particles encountered along the trajectory of the spacecraft during low-altitude flybys (<50 km). Since the sites of origin of the ejected particles lie within a distance from the sub-spacecraft point on the surface comparable to the spacecraft altitude (Postberg et al., 2011b), these in situ samples correspond to feature composition through which the ground track passes (Goode et al., 2021).

Ejecta clouds are produced at airless bodies in the solar system by the continuous bombardment of interplanetary impactors and have been directly detected at the Moon (Horányi et al., 2015), Saturn's moon Enceladus (Spahn et al., 2006; Kempf et al., 2010), as well as at the Galilean moons (Krüger et al., 1999, 2000, 2003; Krivov et al., 2003) by on board dust instruments. In the Jovian system, Jupiter's gravitational focusing enhances both the number density and speed (Colombo et al., 1966; Spahn et al., 2006) of interplanetary impactors, resulting in a flux of impactors onto Europa's icy surface producing  $\sim 10^9$  ejecta  $\text{km}^{-2} \text{s}^{-1}$  for ejecta particles > 200 nm in radius. SUDA will encounter thousands of samples from this ejecta cloud during a typical flyby with a Closest Approach (C/A) altitude <50 km.

While the ejecta cloud for the Moon is asymmetric due to the sporadic impactor sources (Horányi et al., 2015), satellites deep within the gravitational sphere of influence of a massive planet (e.g. Jupiter) are impacted by meteoroids whose orbital parameters are effectively randomized. This results in a nearly isotropic flux onto the moon's surface (Sremčević et al., 2005) where a nearly symmetric ejecta cloud was observed at every Galilean moon on every flyby by the Galileo spacecraft. This allows the ejecta cloud model for Europa to be applied anywhere over the surface.

Ejecta particles enter SUDA and impact a metal target at the back of the instrument at speeds dominated by the spacecraft speed relative to the moon ( $4\text{--}6 \text{ km s}^{-1}$ ) producing a cloud of neutral and ionized material from the target and particle (Postberg et al., 2011b; Kempf et al., 2012; Kempf et al., 2014). The ions at the impact site are separated by an electric field maintained by ion optics and accelerated towards a detector where the time-of-flight (TOF) mass spectra are measured.

SUDA provides precise identification of surface salts on Europa including trace amounts of NaCl and  $\text{MgSO}_4$  preserved in ice materials (Kempf et al., 2012). The recorded spectra from each particle are categorized based on compositional abundances contained in the particle (Hillier et al., 2007; Postberg et al., 2008, 2009). For example, particles rich in salt or organic compounds (Postberg et al., 2018) show distinct characteristics in the mass spectra compared to those from pure water ice. Given the crater depth from interplanetary impactors (Koschny and Grün, 2001), ejecta particles from Europa's surface carry compositional information down to a depth on the order of a few mm (assuming  $10^{-8}$  kg particles impacting Europa at  $20 \text{ km s}^{-1}$ ).

The time series of compositional types (i.e. compositional measurements with associated time stamps) acquired over terrain features on Europa is used to characterize the relative abundances of chemical species belonging to the feature. In this paper, we examine the fourteenth Europa encounter (E14) in the reference tour for Europa Clipper (21F31v4). This flyby has a 35 km altitude closest approach (C/A) point over Thera Macula with a ground-track that passes very near Thrace Macula (Fig. 1 a), which is a typical flyby profile over a young terrain feature in the current tour design. Both of these features are valuable targets for compositional investigation since they likely present up-welled material from beneath the ice crust (Wilson et al., 1997; Mével and Mercier, 2007).

The dark albedo that characterizes Thera and Thrace Macula is indicative of their compositional distinctiveness from the surrounding "background" terrain (Shirley et al., 2010; McCord et al., 2010). We therefore assume material ejected from these features has compositional abundances that result in TOF spectra that are likewise distinct from ejecta originating outside the feature.

It is statistically known (Postberg et al., 2011b; Goode et al., 2021) that most detections originate from within a nadir-projected circle on the surface with a radius equal to the instantaneous spacecraft altitude. This can therefore be used to represent SUDA's footprint showing the approximate spatial resolution as a function of time (Fig. 1 b). It is clear that low-altitude flybys directly over large features enables SUDA to resolve the feature in its detections, such as in the case for Thera Macula. However, small features such as the Dark Band, or adjacent features such as Thrace Macula and Libya Linea, are more difficult to resolve.

Throughout this paper, three simulated compositional types representing the dominant non-ice component of young terrain features (type A), intermediate non-water content (type B), and pure water ice (type C) are assumed to be distributed based on their compositional abundances within a feature. We make no assumptions regarding the specific non-water ice component in young terrain features. It is reasonable to assume that a given feature contains multiple compositional types that contribute to detected ejecta particles. To reflect this, our analysis is based on compositional setups where the fraction of ejecta perceived by SUDA as belonging to a particular compositional type (referred to as  $T_j$  in this paper) in the TOF spectra is defined for a given feature. For example, ejecta originating from Thera Macula may appear as type A 80% of the

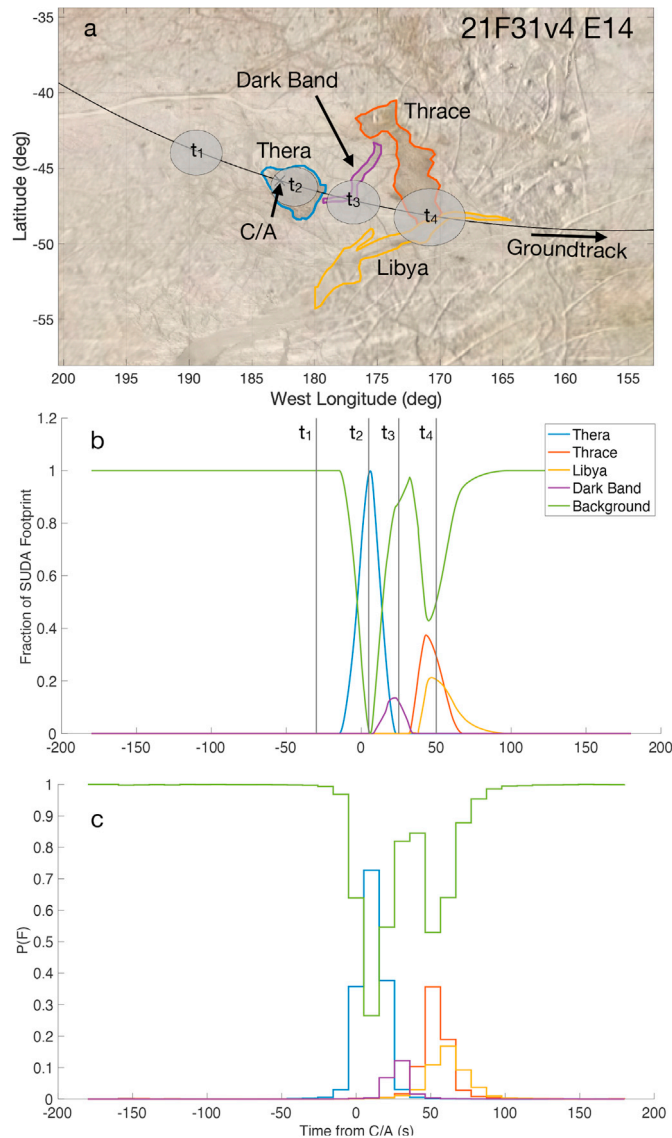


**Fig. 1.** The groundtrack for reference flyby (E14) with a 35 km Closest Approach (C/A) over Thera Macula (panel a) is shown with the nadir-projected circles with radii equal to the instantaneous spacecraft altitude to represent the spatial footprint of SUDA. Four select times along the flyby ( $t_1$ ,  $t_2$ ,  $t_3$ , and  $t_4$ ) show where most of SUDA's detections originate at the select times. The fractions of the instantaneous SUDA footprint occupied by a given feature (panel b) quantifies how features are resolved as a function of time. While most SUDA detections originate from within the footprint, there is still some mixing in the ejecta sites of origin. The small size of the Dark Band within the SUDA footprint makes it difficult to separate from the background. Detections from Thrace Macula at  $t_4$  are mixed with those from Libya. To derive the probability of a detections originating from a feature,  $P(F)$ , Monte Carlo (MC) simulations are applied (panel c) tracking ejecta sites of origin.

time whereas ejecta originating from the background terrain may appear as type C 90% of the time.

## 2. Simulation method

Our simulations employ the model of an ejecta cloud by Krivov et al. (2003) using the parameters given in Table 1. Ejecta particle detections are simulated by a Monte Carlo (MC) method introduced in Goode et al. (2021), except while they considered a single circular feature with one compositional type, we consider unique geological features on Europa with multiple types distributed on the surface. We also apply actual

**Table 1**

Ejecta model parameter values used in this study.

Parameter	Definition	Value
$G_{sil}$	Percentage content of silicate in the surface material	0%
$K_e/K_i$	Percentage of the impactor's kinetic energy imparted to the ejecta	30%
$u_0$	Minimum ejecta speed from the surface	29 m/s
$\gamma$	Slope of the ejecta speed distribution at the surface	2
$\alpha$	Slope of the ejecta size distribution	12/5
$R_m$	Mean radius of Europa	1560.8 km
$\psi_0$	Maximum opening cone angle of the ejecta launch velocities at the surface	30 deg
Size Threshold	Ejecta detection threshold of the instrument	200 nm

Europa Clipper trajectories with SUDA on the reference tour (21F31v4) to simulate detections we expect to see. We assume that the ejecta launch velocity distribution is the same everywhere on the surface of Europa where the only differences between the features are their compositional abundances. Furthermore, we assume that the probability of detection of a type by SUDA depends only on the feature of origin and is not significantly affected by variations in encounter speed.

In a first step, we compile for a given flyby trajectory a profile of expected particle number density from our implementation (Goode et al., 2021) of the Krivov et al. (2003) dust cloud model. With the known velocity and orientation of SUDA we convert this into an average rate of grain detections on SUDA. From this rate we generate a synthetic time series of detections employing Poisson-distributed time intervals between individual detections (Goode et al., 2021). In a second step we generate for each detection a plausible grain velocity vector, drawing random variates from the phase-space distribution of the Krivov et al. (2003) cloud model (Goode et al., 2021). From the latter we can then compute the points of origin for each detected grain. This allows us on a given small segment of the flyby trajectory to infer the probability,  $P(F)$ , that a detected grain originates from inside a certain feature on the surface based on repeating the MC of the flyby for 1000 runs (Fig. 1 c). We run the same flyby trajectory again in a third step where we then assign for all detections from each feature (or region on the surface) a compositional type. These compositional types follow an assumed distribution of compositions corresponding to their feature (or region) of origin. This distribution is fixed but different for young terrain features and background terrain. As a result, we have a MC representation of the whole measurement process for SUDA at a Europa flyby, which we repeat for 50 MC runs. When SUDA carries out its measurement, then only the time series of detections and their compositional types are known. In our simulation we investigate how we can re-derive from this, knowledge of the distribution of compositional types within the surface features as well as the differences in composition between surface features and the background terrain.

### 2.1. Simulating species detection time series

To simulate a stochastic time series of compositional types detected by SUDA along a flyby, we set up an assumed ground-truth for each feature's compositional distribution (Fig. 2). Each ejecta particle is randomly assigned a species designation in the simulation according to the ground-truth distribution for its region of origin. Each compositional type recorded by SUDA forms its own time series of detections (Fig. 3 a). This method assumes the compositional distribution is the same everywhere within the feature boundaries. The goal of this task is to generate a synthetic time series corresponding to an otherwise unknown ground truth. Small features such as the "Dark Band" between Thera and Thrace Macula and the nearby feature, Libya Linea, are included to simulate the effects of their compositional abundances on the time series of SUDA detections due to their close proximity to the features of interest, namely Thera and Thrace Macula.

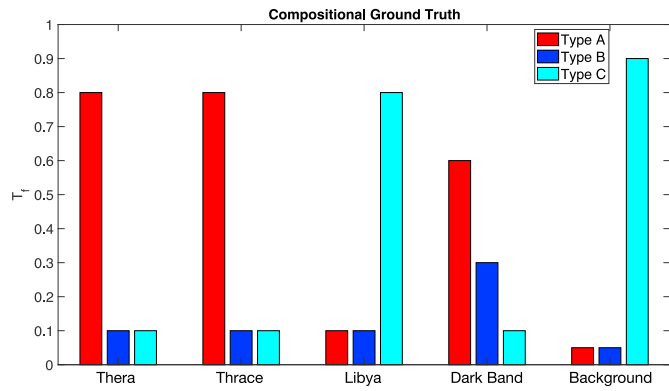


**Fig. 2.** Assumed ground truth setup for compositional abundance ( $T_f$ ) distribution in each feature used in this study. Type A represents high content of non-water ice, type B represents an intermediate content, and type C represents nearly pure water ice. Thera and Thrace Macula are set to be 80% type A given their distinct low albedo in contrast to the background (i.e. surrounding terrain), which is set to 90% type C. The Dark Band between Thera and Thrace along with Libya Linea are set to the compositional ground truth shown to simulate the effect of their material on the time series of compositional detections given their close proximity.

Given the distinctly low albedo of Thera and Thrace Macula, we set  $T_f = 0.8$  for type A (high non-water-ice content),  $T_f = 0.1$  for types B (intermediate mixture) and C (mostly water-ice) for both features. The “background” domain refers to locations on the surface not belonging to any compositionally distinct feature, where  $T_f = 0.9$  for type C and  $T_f =$

0.1 for types A and B in the simulated ground truth. The Dark Band ground truth is simulated as having a lower  $T_f$  for non-water-ice type A ejecta given its higher albedo compared to Thera and Thrace. The Libya Linea ground truth is simulated with  $T_f$  for type C close to that of the background (Fig. 2).

Even in the case where detections are made directly over a compositionally distinct feature, multiple species will be mixed in the time series of detections. This is due to (1) ejecta originating from other compositionally distinct regions reaching the instrument while over the feature (Goode et al., 2021) and (2) the feature itself having more than one compositional type. We now develop a method for associating detected compositional types with surface features to characterize the ground truth of the surface composition.

### 3. Characterizing the composition of surface features using SUDA data

The probability of detections for a distinct compositional type belonging to a feature correlates with proximity to the feature during a flyby. The time series of various compositional types that make up the surface can be divided into subsets of the total detected material giving the detection fractions for each type. If we consider detections very near the feature, such that all detections in a time interval originate exclusively from the feature, then the detection fraction of each compositional type corresponds exactly to the compositional abundances,  $T_f$ , on the surface of the feature. Very far away from the feature, the detection fraction of each compositional type corresponds to the abundances outside the feature. In between these two limits, the relation between compositional detection fraction and proximity to the feature is used to infer the ground truth of compositional distributions within the feature.

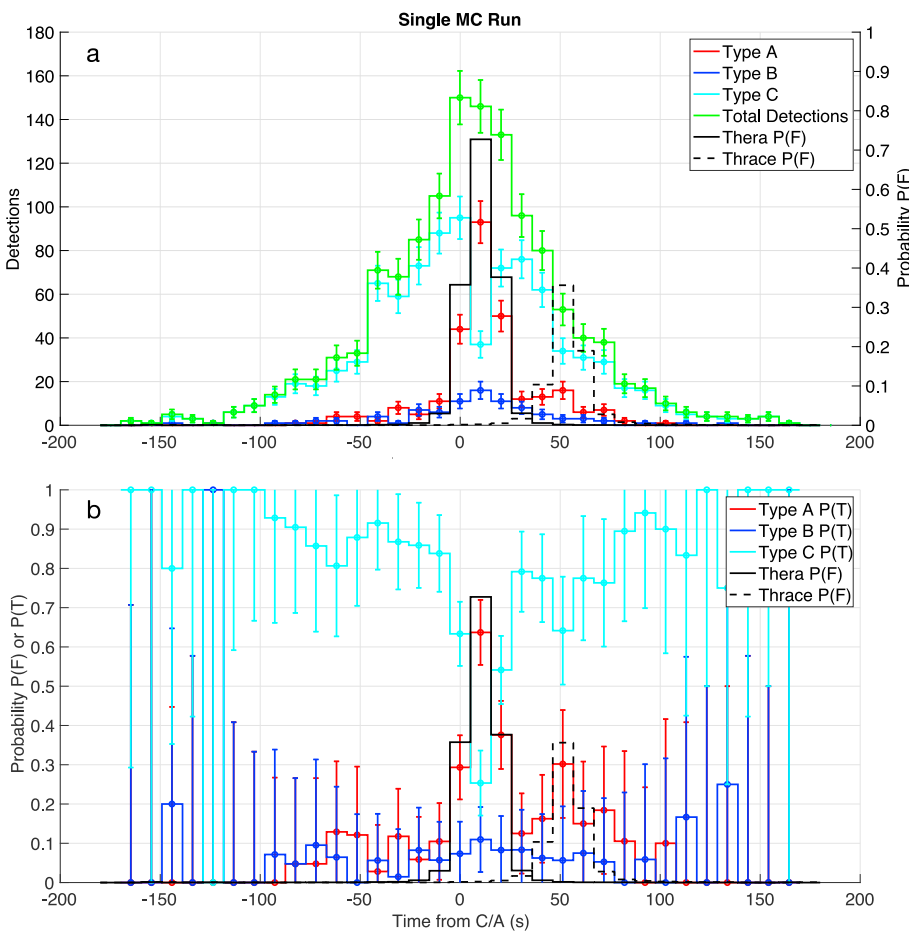


**Fig. 3.** Representative result of a Monte Carlo (MC) simulation of the reference flyby (E14) over Thera Macula. The ground truth consists of three types with abundances that depend on the feature of origin. Using a 10 s time bin, the number of types detected (panel a) is shown. We show the forward-modeled feature probability,  $P(F)$ , (from separate MC trials) in each time bin for Thera and Thrace Macula as a function of time along the flyby. The relative frequency of compositional detections in each time bin is used to compute the empirical probability,  $P(T)$ , of a detected ejecta particle being a given type (panel b). In this case, it is clear that type A (red) detections are associated with Thera and Thrace as probable sites of origin. The compositional ground truth used in this simulation is shown in Fig. 2.

The detection fraction of compositional types in each time bin, which may have contributions from multiple features, is used to compute the empirical probability of a detected particle belonging to a particular compositional type in a given time bin along the flyby,  $P(T)$ , where event  $T$  corresponds to a detection belonging to a given compositional type (Fig. 3 b). The conditional probability of event  $T$  given it originates from a feature,  $P(T|F)$ , is equivalent to the abundance of the compositional type,  $T_f$ , inside the feature. Considering a single feature, the detected particle either originates from the feature (event  $F$ ) or from outside the feature on the surface (event  $F'$ ), such that  $P(F) + P(F') = 1$ . The law of total probability for event  $T$  is written as,

$$P(T) = P(T|F)P(F) + P(T|F')P(F'), \quad (1)$$

or

$$P(T) = (P(T|F) - P(T|F'))P(F) + P(T|F'). \quad (2)$$

Assuming  $P(T|F)$  and  $P(T|F')$  are constant (i.e. the type corresponding to event  $T$  is time-independent), then the probability of a detected particle belonging to a given compositional type depends on the probability of originating from the feature as the following:

$$P(T) = \alpha P(F) + \beta, \quad (3)$$

where  $\alpha = P(T|F) - P(T|F')$  ( $\alpha \in (-1, 1)$ ),  $\beta = P(T|F')$  ( $\beta \in (0, 1)$ ), and  $\alpha +$

$\beta = P(T|F)$  gives the abundance of the detected ejecta compositional type inside the feature. With  $P(F)$  forward-modeled from the MC simulations and  $P(T)$  computed from the time series of compositional detections by SUDA, the coefficients,  $\alpha$  and  $\beta$ , are estimated by a least squares fit to the data (Fig. 4 a and b).

The time series data from the flyby are used to plot  $P(T)$  versus  $P(F)$ . For Thera Macula (Fig. 4 a), the trend clearly shows a dependence of  $P(T)$  on  $P(F)$  for type A and C where we can fit Eq. (3) to data acquired by SUDA after a flyby. The positive slope ( $\alpha > 0$ ) of the fit for type A indicates that Thera is contributing this type to SUDA's detections, which is consistent with the compositional type being more abundant inside the feature than outside the feature. On the other hand, the negative slope ( $\alpha < 0$ ) of the type C fit indicates that it is mostly contributed to SUDA's detections from outside Thera. The lack of dependence for type B ( $\alpha \approx 0$ ) clearly indicates that it is found in similar abundances outside and inside the feature. The sum of the coefficients from the fit to the data gives the abundances of each compositional type in the feature (Fig. 4 c and d).

Using the trends in the time series data returned by SUDA versus MC-derived feature of origin probabilities, the compositional abundance estimate agrees well with the otherwise unknown ground truth used in the simulation of flyby E14 in the reference tour design. While Fig. 4 a and b are representative results from a single MC run, the compositional abundance estimate shown in Fig. 4 c and d are averaged results from 50 MC runs where the error bars are the  $1\sigma$  deviations in the MC results. The

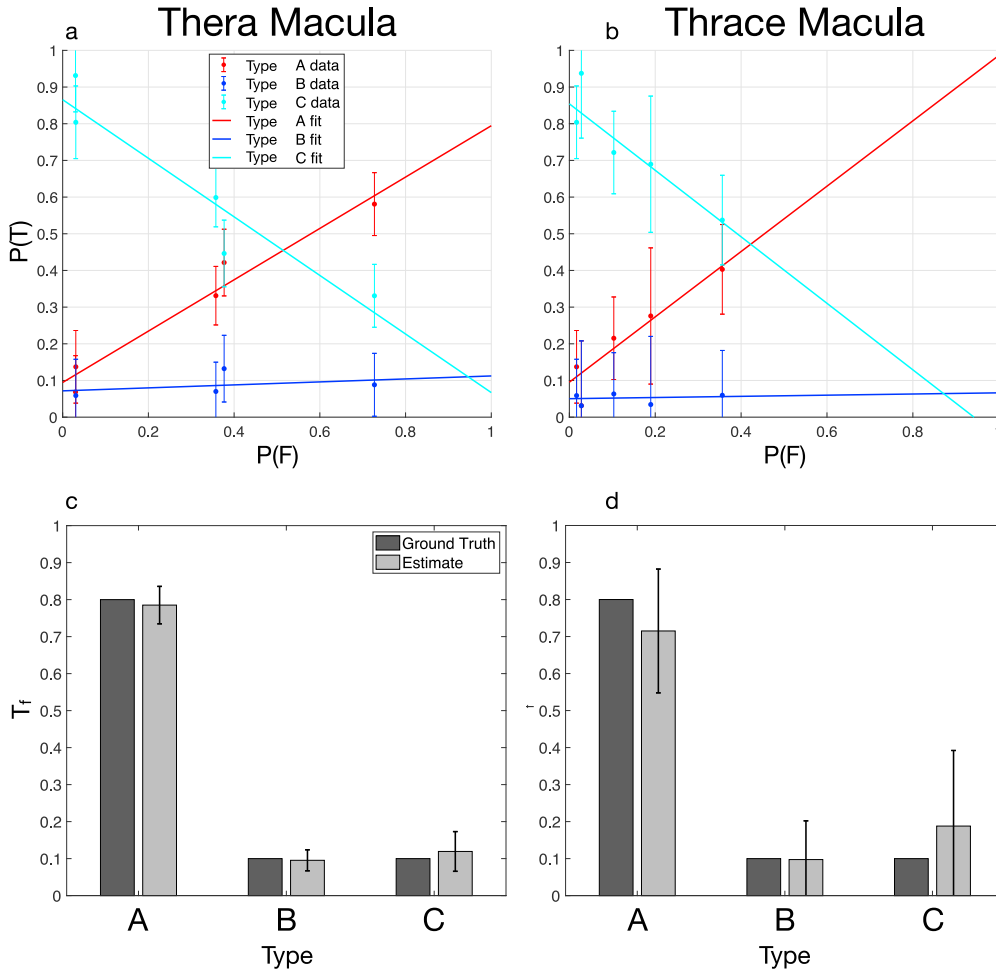


**Fig. 4.** Probability of compositional type detection,  $P(T)$ , versus feature origin probability,  $P(F)$  (panels a and b) from a representative single MC run are plotted to show a correspondence of the feature with each type. The vertical bars for the data show the fractional uncertainty based on the Poisson distribution. The compositional abundance estimate ( $T_f$  in panels c and d) is computed using the coefficients of the fits. The vertical lines on the bar plots show the  $1\sigma$  deviation of 50 MC results. Ground truth used in the simulation is shown for comparison; however, this information is not known a priori for this analysis.

compositional abundance estimates are more precise and accurate for Thera than for Thrace on this flyby trajectory due to the less favorable ground track geometry for the latter feature. Since the spacecraft passes directly over Thera while only passing near the edge of Thrace, the maximum feature probability,  $P(F)$ , is lower with fewer detected ejecta particles originating from Thrace. While a trend can still be seen for Thrace in  $P(T)$  versus  $P(F)$  (Fig. 4 b), the data are of lower quality for the least-squares fit used to estimate the compositional abundance from the coefficients of Eq. (3).

### 3.1. Varying flyby parameters

C/A position for better flyby geometry with respect to Thrace Macula. The quality of the compositional abundance estimate,  $T_f$ , for Thrace is improved compared to that of the original flyby. The  $T_f$  estimate for Thera Macula is both less accurate and has a larger  $1\sigma$  deviation in the MC runs. Since only one realisation of the estimate will be computed

during the mission, the  $P(T)$  versus  $P(F)$  trend (from a single MC run) indicate the lack of precision that can be assumed about the compositional abundance ground truth estimate.

Since the flyby trajectory in the reference tour has favorable geometry for acquiring the ground truth of Thera Macula but not for Thrace Macula, we adjust the flyby so that the C/A is instead placed over Thrace to examine the effect on compositional abundance estimate accuracy. The nominal E14 flyby is adjusted by moving the C/A point East by  $10^\circ$  and South by  $1^\circ$  (Fig. 5). The groundtrack passes directly over Thrace Macula while passing North of Thera. The species abundance estimate for Thrace is now more precise and accurate while that of Thera is degraded compared to the nominal (i.e. original) case. This demonstrates the importance of overflying the feature in order to acquire accurate ground truth estimates.

The quality of the species abundance estimate also depends on altitude since there are fewer detections due to the decreasing ejecta cloud density with altitude and the fact that species are more mixed with sites

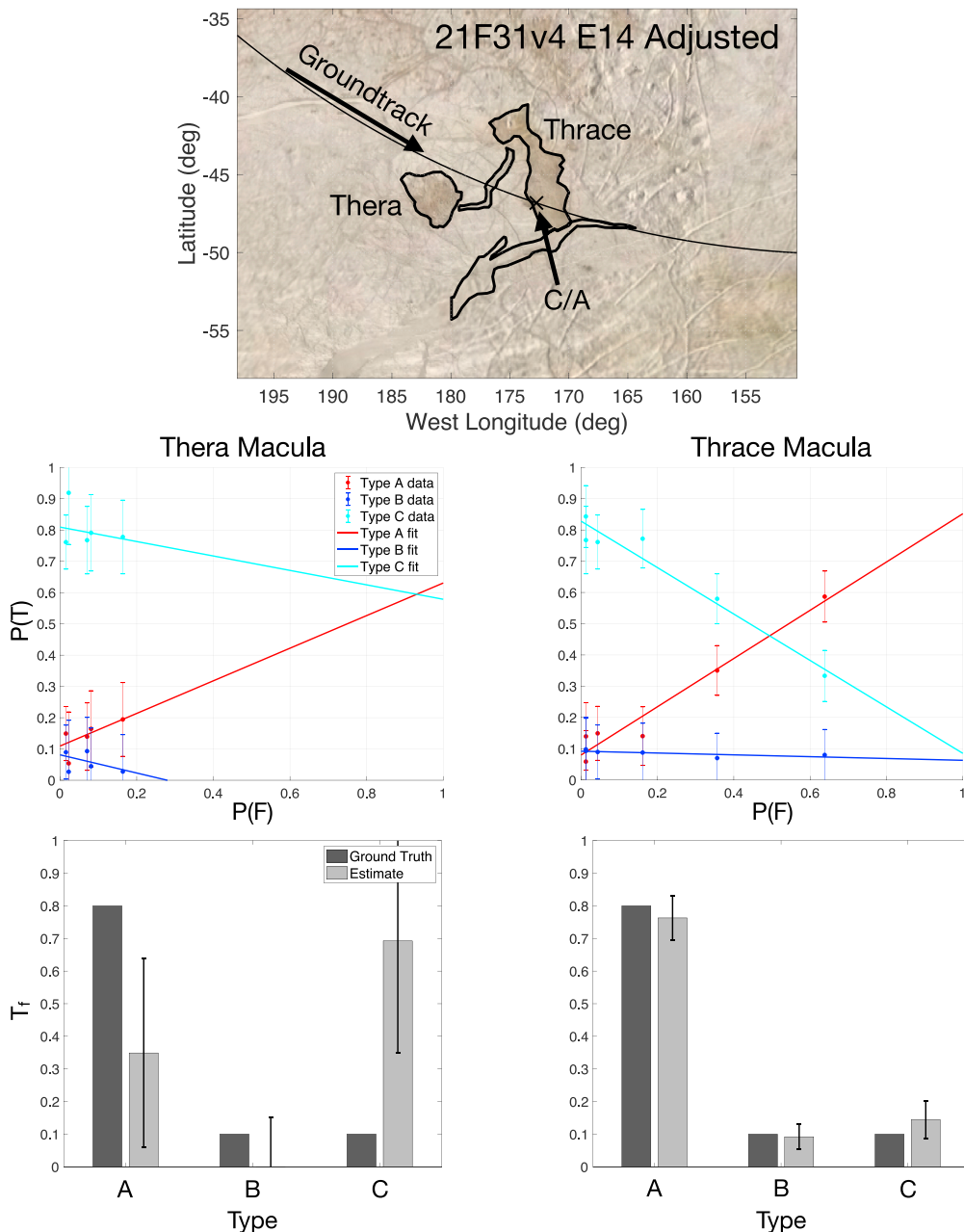


Fig. 5. Same situation as in Fig. 4 but with an adjusted.

of origin further away from the spacecraft groundtrack (Goode et al., 2021). We adjust the C/A altitude up from 35 km to 50 and 100 km on the original trajectory and compute the species abundance estimate for Thera Macula (Fig. 6). The quality of the species abundance estimate results at 50 km C/A is similar to that at the nominal 35 km, albeit with a slightly larger  $1\sigma$  deviation from the MC runs. At 100km C/A, on the other hand, the species abundance estimate results are practically unusable. The reason for this is clear from the  $P(T)$  versus  $P(F)$  (Fig. 6 c) where the maximum feature probability is much lower and the relative species number uncertainties are larger due to the low number of detections.

### 3.2. Varying ground truth

Prior to each flyby during the Europa Clipper mission, we will not know a priori how compositionally distinct, if at all, a feature will be as seen in SUDA's data. It is important that the compositional abundance estimate reflect the actual ground truth, or at the very least not produce misleading results if the data are inadequate for computing an accurate result. In the adjusted case above, the trend in  $P(T)$  versus  $P(F)$  for Thera shows that the species abundance estimates should not be trusted. In other words, the quality of the estimate during the mission is evident based on the trend in the data.

To examine cases where the ground truth can vary from what we expect as stated in section 2 and shown in Fig. 2, we lower the type A abundance in the simulated Thera Macula ground truth (exchanging non-water ice type for more water ice type) and compute the compositional abundance estimate from MC runs of the nominal E14 flyby in the reference tour design while leaving the ground truth for the rest of the features unaltered. In the case where  $T_f$  for type A from Thera is 0.5, the

slope of  $P(T)$  versus  $P(F)$  (Fig. 7 a) is less than in the case of higher abundance, although the still positive slope indicates a correspondence of the feature with this type (i.e. the type is clearly coming from this feature). The subsequent compositional abundance estimate agrees well with the ground truth (Fig. 7 b). Setting  $T_f$  for type A to 0.1 makes the compositional distribution of Thera Macula nearly identical to that of the background terrain (i.e. the feature is not compositionally distinct). The approximately flat slopes of the fit lines in the  $P(T)$  versus  $P(F)$  trend (Fig. 7 c) indicate little to no correspondence of the feature with any detected compositional types resulting in a compositional abundance estimate that also agrees well with the ground truth, where type C (i.e. pure water ice) dominates the surface composition of Thera Macula.

### 4. Summary and conclusions

The time series of compositional types obtained by SUDA during flybys over terrain features provides a direct estimate of the compositional abundance ground truth. MC simulations, based on the dynamical phase space of the ejecta particles (Krivov et al., 2003; Goode et al., 2021), that are performed on the known trajectory for the spacecraft with SUDA are used to compute the probability of a detection originating from a feature,  $P(F)$ , during a time interval along a flyby. Compositional detection times obtained on the flyby are binned to compute the empirical probability of a compositional type detection,  $P(T)$ , during the same time interval along the flyby. Using the law of total probability, we apply data obtained by SUDA to acquire the compositional ground truth for a feature on the surface of Europa via the  $P(T)$  versus  $P(F)$  relationship.

This method is effective for whatever compositional abundances that may exist in a feature along the flyby trajectory and will also work if the

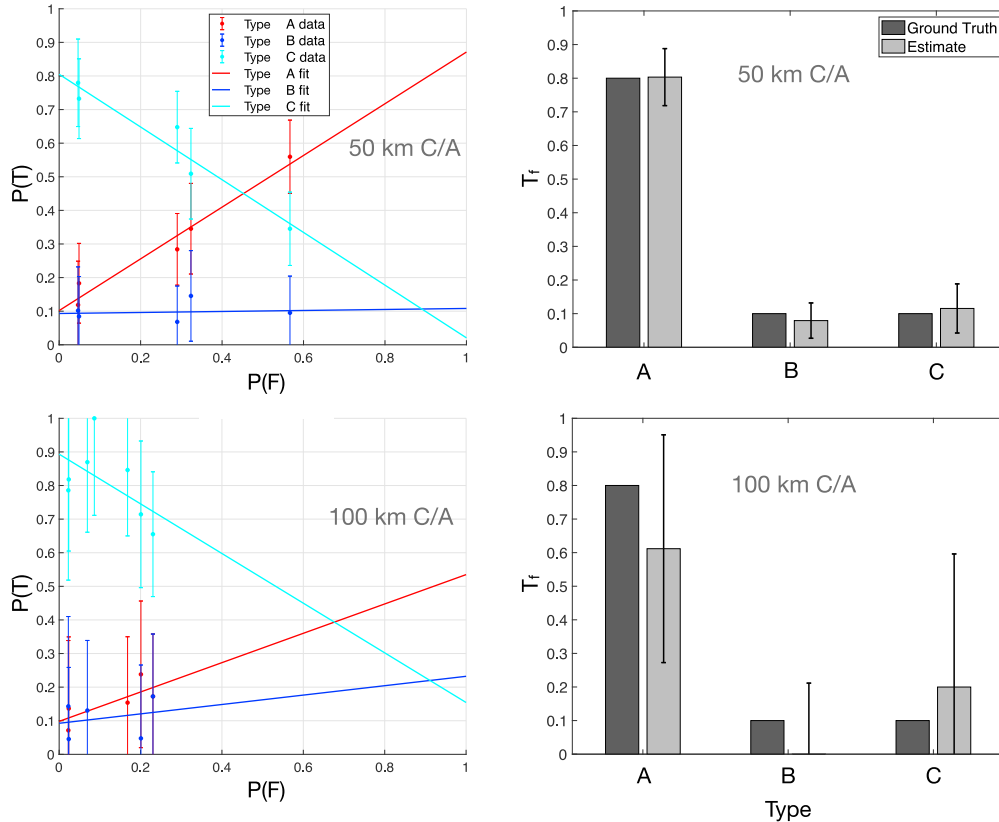
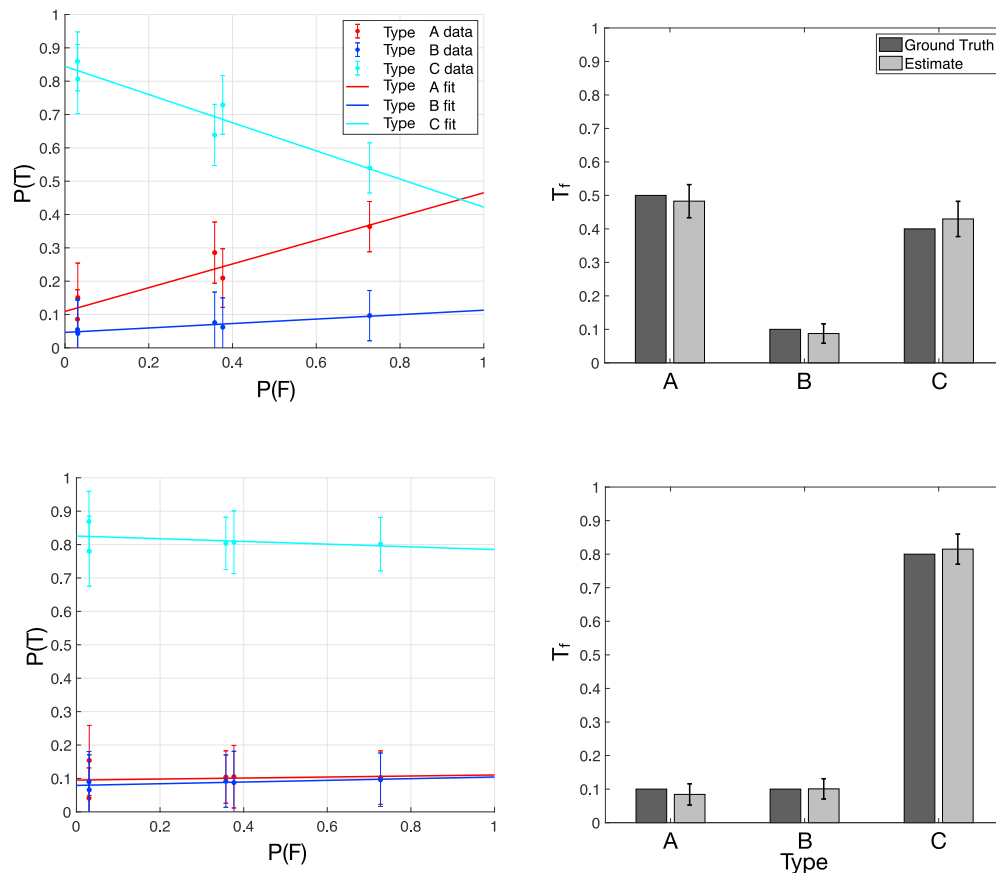


Fig. 6. Compositional abundance estimates for Thera Macula with adjusted C/A altitude at 50 and 100 km on E14. The data for the  $P(T)$  versus  $P(F)$  trend (shown from one run) decreases in quality with increasing altitude resulting in a less accurate compositional abundance estimate (averaged from 50 MC runs) at 100 km C/A over the feature.



**Fig. 7.** Various compositional ground truths for Thera Macula and the resulting compositional abundance estimates:  $T_f$ . The data for the  $P(T)$  versus  $P(F)$  trend (shown from one run) show clear trends that correspond with the given compositional ground truth. The resulting accuracy of the  $T_f$  estimate is independent of ground truth.

feature is not compositionally distinct from the surrounding terrain. As expected, compositional type abundance estimates for the ejecta compositional ground truth of a terrain feature is most precise and accurate for low altitude flybys directly over the feature. If the TOF spectra indicate molar abundances of chemical compounds, the ejecta compositional type abundance,  $T_f$ , computed here can be used to infer the molar abundance on the feature's surface. The ground truth estimates provided by SUDA can be combined with other methods of measuring surface composition (e.g. near infrared and UV spectroscopy) to provide a holistic understanding of the nature of geological terrain features and the knowledge they provide regarding Europa's habitability.

#### Author statement

**William Goode:** Conceptualization, Methodology, Simulation and Data Analysis, Writing-Original draft preparation, Writing-Reviewing and Editing, Writing-Revising Manuscript. **Sascha Kempf:** Conceptualization, Methodology, Writing-Reviewing and Editing, Writing-Revising Manuscript. **Juergen Schmidt:** Writing-Reviewing and Editing, Writing-Revising Manuscript.

#### Declaration of competing interest

The authors declare the following financial interests/personal relationships which may be considered as potential competing interests: William Goode reports financial support was provided by NASA.

#### Data availability

Data will be made available on request.

#### Acknowledgements

**Funding:** This work was supported by NASA through the Europa Clipper Project.

The authors would like to thank Alex Doner for helpful discussions in the development of the concepts in the paper. We also thank Morgan Cable and Samantha Trumbo for valuable feedback on the manuscript.

#### References

- Brown, M.E., Hand, K.P., 2013. Salts and radiation products on the surface of Europa. *Astron. J.* 145 (4), 110.
- Carlson, R., Anderson, M., Mehlman, R., Johnson, R., 2005. Distribution of hydrate on Europa: further evidence for sulfuric acid hydrate. *Icarus* 177 (2), 461–471.
- Chyba, C.F., Phillips, C.B., 2001. Possible ecosystems and the search for life on Europa. *Proc. Natl. Acad. Sci. USA* 98 (3), 801–804.
- Colombo, G., Lautman, D.A., Shapiro, I.I., 1966. The earth's dust belt: fact or fiction?, 2, gravitational focusing and Jacobi capture. *J. Geophys. Res.* 71, 5705–5717.
- Dalton, J.B., 2007. Linear mixture modeling of Europa's non-ice material based on cryogenic laboratory spectroscopy. *Geophys. Res. Lett.* 34 (21).
- Figueredo, P.H., Greeley, R., 2004. Resurfacing history of Europa from pole-to-pole geological mapping. *Icarus* 167 (2), 287–312.
- Goode, W., Kempf, S., Schmidt, J., 2021. Detecting the surface composition of geological features on Europa and Ganymede using a surface dust analyzer. *Planet. Space Sci.* 208, 105343.
- Hand, K.P., Brown, M.E., 2013. Keck II observations of hemispherical differences in H<sub>2</sub>O on Europa. *Astrophys. J. Lett.* 766 (2), L21.
- Hand, K.P., Carlson, R.W., Chyba, C.F., 2007. Energy, chemical disequilibrium, and geological constraints on Europa. *Astrobiology* 7 (6), 1006–1022.

- Hillier, J.K., Green, S.F., McBride, N., Schwanethal, J.P., Postberg, F., Srama, R., Kempf, S., Moragas-Klostermeyer, G., McDonnell, J.A.M., Grün, E., 2007. The composition of Saturn's E ring. *Mon. Not. Roy. Astron. Soc.* 377 (4), 1588–1596.
- Horányi, M., Szalay, J.R., Kempf, S., Schmidt, J., Grün, E., Srama, R., Sternovsky, Z., 2015. A permanent, asymmetric dust cloud around the Moon. *Nature* 522 (7556), 324–326.
- Kempf, S., Beckmann, U., Schmidt, J., 2010. How the Enceladus dust plume feeds Saturn's E ring. *Icarus* 206 (2), 446–457.
- Kempf, S., Srama, R., Grün, E., Mocker, A., Postberg, F., Hillier, J.K., Horányi, M., Sternovsky, Z., Abel, B., Beinsen, A., Thissen, R., Schmidt, J., Spahn, F., Altobelli, N., 2012. Linear high resolution dust mass spectrometer for a mission to the galilean satellites. *Planet. Space Sci.* 65 (1), 10–20.
- Kempf, S., Altobelli, N., Briois, C., Cassidy, T., Grün, E., Horanyi, M., Postberg, F., Schmidt, J., Shasharina, S., Srama, R., Sternovsky, Z., 2014. Compositional mapping of Europa's surface with a dust mass spectrometer. *LPI Contrib. No. 1774*, 4052.
- Koschny, D., Grün, E., 2001. Impacts into ice-silicate mixtures: crater morphologies, volumes, depth-to-diameter ratios, and yield. *Icarus* 154 (2), 391–401. <https://doi.org/10.1006/icar.2001.6707>.
- Krivov, A.V., Sremčević, M., Spahn, F., Dikarev, V.V., Kholshvnikov, K.V., 2003. Impact-generated dust clouds around planetary satellites: spherically symmetric case. *Planet. Space Sci.* 51, 251–269.
- Krüger, H., Krivov, A., Hamilton, D., Grün, E., 1999. Detection of an impact-generated dust cloud around Ganymede. *Nature* 399, 558–560.
- Krüger, H., Krivov, A.V., Grün, E., 2000. A dust cloud of Ganymede maintained by hypervelocity impacts of interplanetary micrometeoroids. *Planet. Space Sci.* 48, 1457–1471.
- Krüger, H., Krivov, A.V., Sremčević, M., Grün, E., 2003. Impact-generated dust clouds surrounding the Galilean moons. *Icarus* 164, 170–187.
- Lam, T., Buffington, B., Campagnola, S., 2018. A robust mission tour for NASA's planned Europa Clipper mission. In: 2018 Space Flight Mechanics Meeting. AIAA SciTech Forum.
- Ligier, N., Poulet, F., Carter, J., Brunetto, R., Gourgeot, F., 2016. VLT/SINFONI observations of Europa: new insights into the surface composition. *Astron. J.* 151 (6), 163.
- Marais, D.J.D., Nuth, J.A., Allamandola, L.J., Boss, A.P., Farmer, J.D., Hoehler, T.M., Jakosky, B.M., Meadows, V.S., Pohorille, A., Runnegar, B., Spormann, A.M., 2008. The NASA astrobiology roadmap. *Astrobiology* 8 (4), 715–730. <https://doi.org/10.1089/ast.2008.0819>. ISSN 1531-1074.
- Marion, G.M., Fritsen, C.H., Eicken, H., Payne, M.C., 2003. The search for life on Europa: limiting environmental factors, potential habitats, and Earth analogues. *Astrobiology* 3 (4), 785–811.
- McCord, T.B., Hansen, G.B., Fanale, F.P., Carlson, R.W., Matson, D.L., Johnson, T.V., Smythe, W.D., Crowley, J.K., Martin, P.D., Ocampo, A., Hibbitts, C.A., Granahan, J.C., Team, t.N., 1998. Salts on Europa's surface detected by Galileo's near infrared mapping spectrometer. *Science* 280 (5367), 1242–1245.
- McCord, T.B., Hansen, G.B., Matson, D.L., Johnson, T.V., Crowley, J.K., Fanale, F.P., Carlson, R.W., Smythe, W.D., Martin, P.D., Hibbitts, C.A., Granahan, J.C., Ocampo, A., 1999. Hydrated salt minerals on Europa's surface from the Galileo near-infrared mapping spectrometer (NIMS) investigation. *J. Geophys. Res.: Planets* 104 (E5), 11827–11851.
- McCord, T.B., Hansen, G.B., Combe, J.-P., Hayne, P., 2010. Hydrated minerals on Europa's surface: an improved look from the Galileo NIMS investigation. *Icarus* 209 (2), 639–650.
- Mével, L., Mercier, E., 2007. Large-scale doming on Europa: a model of formation of Thera Macula. *Planet. Space Sci.* 55 (7), 915–927.
- Pappalardo, R.T., Sullivan, R.J., 1996. Evidence for separation across a gray band on Europa. *Icarus* 123 (2), 557–567.
- Pappalardo, R.T., Head, J.W., Greeley, R., Sullivan, R.J., Pilcher, C., Schubert, G., Moore, W.B., Carr, M.H., Moore, J.M., Belton, M.J.S., Goldsby, D.L., 1998. Geological evidence for solid-state convection in Europa's ice shell. *Nature* 391 (6665), 365–368.
- Postberg, F., Kempf, S., Hillier, J., Srama, R., Green, S., McBride, N., Grün, E., 2008. The E-ring in the vicinity of Enceladus: II. probing the moon's interior—the composition of E-ring particles. *Icarus* 193 (2), 438–454.
- Postberg, F., Kempf, S., Schmidt, J., Brilliantov, N., Beinsen, A., Abel, B., Buck, U., Srama, R., 2009. Sodium salts in E-ring ice grains from an ocean below the surface of Enceladus. *Nature* 459, 1098–1101.
- Postberg, F., Grün, E., Horanyi, M., Kempf, S., Krüger, H., Schmidt, J., Spahn, F., Srama, R., Sternovsky, Z., Trieloff, M., 2011a. Compositional mapping of planetary moons by mass spectrometry of dust ejecta. *Planet. Space Sci.* 59 (14), 1815–1825.
- Postberg, F., Schmidt, J., Hillier, J., Kempf, S., Srama, R., 2011b. A salt-water reservoir as the source of a compositionally stratified plume on Enceladus. *Nature* 474, 620–622.
- Postberg, F., Khawaja, N., Abel, B., Choblet, G., Glein, C.R., Gudipati, M.S., Henderson, B.L., Hsu, H.-W., Kempf, S., Klenner, F., Moragas-Klostermeyer, G., Magee, B., Nölle, L., Perry, M., Reviol, R., Schmidt, J., Srama, R., Stolz, F., Tobie, G., Trieloff, M., Waite, J.H., 2018. Macromolecular organic compounds from the depths of Enceladus. *Nature* 558 (7711), 564–568.
- Prockter, L.M., Shirley, J.H., Dalton, J.B., Kamp, L.W., 2017. Surface composition of pull-apart bands in Argadnel Regio, Europa: evidence of localized cryovolcanic resurfacing during basin formation. *Icarus* 285, 27–42.
- Schmidt, B.E., Blankenship, D.D., Patterson, G.W., Schenk, P.M., 2011. Active formation of 'chaos terrain' over shallow subsurface water on Europa. *Nature* 479 (7374), 502–505.
- Shirley, J.H., Dalton, J.B., Prockter, L.M., Kamp, L.W., 2010. Europa's ridged plains and smooth low albedo plains: distinctive compositions and compositional gradients at the leading side–trailing side boundary. *Icarus* 210 (1), 358–384.
- Spahn, F., Schmidt, J., Albers, N., Hörning, M., Makuch, M., Seiß, M., Kempf, S., Srama, R., Dikarev, V., Helfert, S., Moragas-Klostermeyer, G., Krivov, A.V., Sremčević, M., Tuzzolino, A.J., Economou, T., Grün, E., 2006. Cassini dust measurements at Enceladus and implications for the origin of the E-ring. *Science* 311, 1416–1418.
- Sremčević, M., Krivov, A.V., Krüger, H., Spahn, F., 2005. Impact-generated dust clouds around planetary satellites: model versus Galileo data. *Planet. Space Sci.* 53, 625–641.
- Trumbo, S.K., Brown, M.E., Hand, K.P., 2019. Sodium chloride on the surface of Europa. *Sci. Adv.* 5 (6), eaaw7123.
- Trumbo, S.K., Brown, M.E., Hand, K.P., 2020. Endogenic and exogenic contributions to visible-wavelength spectra of Europa's trailing hemisphere. *Astron. J.* 160 (6), 282.
- Trumbo, S.K., Becker, T.M., Brown, M.E., Denman, W.T.P., Molyneux, P., Hendrix, A., Retherford, K.D., Roth, L., Alday, J., 2022. A new UV spectral feature on Europa: confirmation of NaCl in leading-hemisphere chaos terrain. *Planetary Sci. J.* 3 (2), 27.
- Wilson, L., Head, J.W., Pappalardo, R.T., 1997. Eruption of lava flows on Europa: theory and application to Thera Macula. *J. Geophys. Res.: Planets* 102 (E4), 9263–9272.